THE UNIVERSITY OF
WARWICK

A Genetic Algorithm Method for Optical Wireless Channel Control

Matthew D. Higgins, Roger J. Green, *Senior Member, IEEE,* and Mark S. Leeson, *Senior Member, IEEE*

Abstract—A genetic algorithm controlled multispot transmitter is proposed as an alternative approach to optimising the power distribution for single element receivers in fully diffuse mobile indoor optical wireless communication systems. By specifically tailoring the algorithm, it is shown that by dynamically altering the intensity of individual diffusion spots, a consistent power distribution, with negligible impact on bandwidth and rms delay spread, can be created in multiple rooms independent of reflectivity characteristics and user movement patterns. This advantageous adaptability removes the need for bespoke system design, aiming instead for the use of a more cost effective, optimal transmitter and receiver capable of deployment in multiple scenarios and applications. From the simulations conducted it is deduced, that implementing a receiver with a FOV = 55° in conjunction with either of two notable algorithms, the dynamic range of the rooms, referenced against the peak received power, can be reduced by up to 26% when empty, and furthermore to within 12% of this optimised case when user movement perturbs the channel.

Index Terms—Genetic algorithm, optical communication, wireless LAN.

I. INTRODUCTION

ONE of the most challenging design aspects of an indoor optical wireless (OW) system, using an infrared (IR) carrier, is overcoming the limitations imposed by the transmission channel. Conventional diffuse configurations, pioneered by Gfeller [1], suffer from intersymbol interference (ISI), wide ranging levels of received power throughout the room and intense quantities of IR ambient radiation [2]. These channel characteristics inhibit the ability to provide high performance OW systems that meet the needs of today's growing demand for mobile multimedia device connectivity. Furthermore, the transmission channel characteristics are dependent upon the room size, stationary and moving objects, material properties of every surface the radiation is incident upon, and the number and type of illumination sources present [3], such that a single system design may have different performance capabilities when implemented in different locations.

To overcome these performance issues, research in the field has led to several possible solutions. Quasi-diffuse configurations employing multispot diffusion (MSD) and diversity receivers [4] improve the bandwidth and ambient noise rejection through the use of an array of photodetector's coupled to either, a single imaging lens [5], or several optical concentrators [6]. Implementation of automatic gain control (AGC) can compensate for the variations in received power at different positions within the room [7]. Modulation techniques such as trellis-coded pulse-position modulation [8], and amplitude shift key digital demodulation [9] are capable of mitigating the effects of ISI, and noise from fluorescent lamps, respectively. More recently the use of *intelligent* techniques have been shown to be beneficial, using neural networks and pattern recognition wavelet analysis to overcome channel induced distortion [10]. Following this, a modified genetic algorithm (GA), based on simulated annealing [11], has been shown to produce highly optimised computer generated holograms, reducing the variation in received power distribution [12], [13].

The most practical OW system architecture is the cellular approach, where a given room has a transceiver base station linked to the backbone network. It is presumed that there are multiple end users in the cell, each with a battery powered portable OW receiver, such as mobile phone, laptop or PDA. Therefore whilst the application of each of the aforementioned techniques has respective performance merits compared to a conventional diffuse OW system, one has to weigh these benefits against the added complexity, cost and physical size of each receiver within the system. This is especially apparent when the number of receivers becomes large, as the cost overhead of a system, will be influenced more by the number of receivers, than the single base station.

In this paper a GA controlled MSD transmitter is proposed, but instead of pairing it with a diversity receiver, a simpler single element receiver is implemented. It will be shown that the GA can dynamically optimise the power distribution for multiple stationary and mobile users within multiple environments, by controlling the power of each diffusion spot. This advantageous adaptability, independent of environmental characteristics and user movement patterns, removes the need for bespoke system design and allows for easier system deployment increasing end user friendliness. Moreover the ability to produce a consistent power distribution at all locations within multiple environments contributes towards uniform system performance characteristics. These performance characteristics then become less dependent upon the ACG capabilities of the receiver, as the transmitter becomes responsible for maximising the signal to noise ratio (SNR) and data rate. The inevitable trade off in the work presented here is the lack of substantial bandwidth gains compared to implementing diversity receivers, but in applications where mobility and cost are paramount, this method aid in the design of an optimum, standardised receiver design realisable for mass product integration.

The remainder of this paper is organised as follows. Section

The authors are with the Department of Engineering, University of Warwick, Coventry, CV4 7AL, UK.
E-mail: {m.higgins, roger.green, mark.leeson}@warwick.ac.uk

II briefly overviews the general system model, applicable transmitter techniques, and impulse response definitions. Section III introduces the channel model theory followed by section IV detailing the GA implementation. Section V provides the results and associated analysis of using the proposed GA. Concluding remarks are presented in section VI.

II. System Model

A. Source, Receiver and Reflector Model

We define our system environment to be an arbitrary indoor rectangular room enclosing a transmitter capable of firstly forming a diffusion spot geometry upon the ceiling and secondly, that each spot intensity can be dynamically and independently controlled. To the best of the authors' knowledge, holographic diffusers [14], whilst being capable of generating predefined spot intensities and/or geometries, such as uniform, diamond or line-strip [15], have static characteristics removing its suitability for the work presented here.

Multiple optical sources [16] allow for any spot pattern geometry to be installed on the ceiling of the room, and whilst it is possible to control the distribution of emitted radiation from each source though the use of lenses or other diffuser techniques [17], traditionally the optical source is a LED, which emits radiation with a generalised Lambertian radiation intensity pattern [18]. Dynamic control of an individual spot intensity is also possible. The installation of multiple optical sources may seem 'bespoke', but the use of white LEDs which not only act as transmission sources, also serve to illuminate the environment, and have beneficial properties such as low power consumption, heat dissipation and cost.

A 2-D vertical cavity surface emitting Laser diode (VCSEL) or resonant cavity LED (RCLED) array, flip-chip bonded to CMOS driver circuitry, allows for a highly-integrated transmitter solution [19], [20]. The driver circuitry is capable of controlling each element's emitted power, along with any other signal processing techniques currently realisable in CMOS. Furthermore, it is possible to integrate beam shaping and steering optics, that can control the position of each of the resultant projected spots on the ceiling, which will then be reflected, according to the reflection properties of the ceiling.

Assuming that the majority of surfaces in our environment exhibit a fully diffuse, as supposed to specular [21]–[23], reflection characteristic that can be described by Lambert's reflection model [24], we can apply the following simplification. Regardless of whether the transmitter is composed of multiple optical sources or a 2-D VCSEL/RCLED array, the resultant diffusion spots on the ceiling will exhibit a Lambertian radiation intensity pattern, and therefore from this point onwards, each of the I diffusion spots on the ceiling will themselves be considered independent sources $\mathcal{S}_i$. The only error induced with this assumption is a delay and propagation loss between the emitting element of an 2-D VCSEL/RCLED array and the diffusion spot position. In an arbitrary room, the number of possible transmitter and diffusing spot positions is essentially infinite, and so this assumption also serves to simplify our argument for using the GA whilst maintaining generality to the application. Referring to figure 1, each source

$\mathcal{S}_i$ will therefore have an associated position vector $\mathbf{r}_{\mathcal{S}_i}$, unit length orientation vector $\hat{\mathbf{n}}_{\mathcal{S}_i}$, power $P_{\mathcal{S}_i}$ and uniaxial symmetric, with respect to $\hat{\mathbf{n}}_{\mathcal{S}_i}$, Lambertian radiation intensity profile $R(\phi)$ given by

$$R(\phi) = \frac{n+1}{2\pi} P_{\mathcal{S}_i} \cos^n(\phi) \qquad \text{for } \theta \in [-\pi/2, \pi/2] \quad (1)$$

Where the mode number, $n = 1$ for a pure Lambertian diffuser, such as the ceiling, and $n > 1$ for a diffusion pattern from an LED with higher directionality.

The aim of this work is to control the power distribution of radiation, enabling the use of a single optimal receiver design at all locations in multiple locations. Therefore, for a given environment we model the existence of J single element receivers $\mathcal{R}_j$. Knowing that receivers $\mathcal{R}_j$ and $\mathcal{R}_{j+1}$ are of the same design, we can simultaneously simulate and readily interchange between describing a system with J receivers at multiple locations and a system with one receiver at J locations. To attain a highly detailed system model, we set $J = 1024$ and uniformly distributed the position vectors $\mathbf{r}_{\mathcal{R}_j}$ of the receivers $\mathcal{R}_j$ over the width x, length y, at a height $z = 1\text{m}$. Each receiver has a vertical orientation vector $\hat{\mathbf{n}}_{\mathcal{R}_j}$, active optical collection area $A_{\mathcal{R}_j}$ and a field of view $FOV_{\mathcal{R}_j}$ defined as the maximum uniaxial symmetric incident angle of radiation with respect to $\hat{\mathbf{n}}_{\mathcal{R}_j}$, that will generate a current in the photodiode. As we have assumed all surfaces within the environment exhibit Lambertian reflection characteristics, which are independent of the angle of the incident radiation, we follow the technique described in [25], and partition all surfaces into L elements $\mathcal{E}_l$ with position $\mathbf{r}_{\mathcal{E}_l}$, orientation $\hat{\mathbf{n}}_{\mathcal{E}_l}$, and size $A_{\mathcal{E}_l} = 1/\Delta A^2 (\text{m}^2)$ where ΔA is the desired number of elements per meter. A given element will sequentially behave, firstly as a receiver $\mathcal{E}_l^{\mathcal{R}}$ with a hemispherical FOV, for which we can determine the received power $P_{\mathcal{E}_l}$, and secondly as a source $\mathcal{E}_l^{\mathcal{S}}$, with a radiation intensity profile $R(\phi)$ is given by (1) setting $n = 1$ and $P_{\mathcal{S}_i} = \rho_{\mathcal{E}_l} P_{\mathcal{E}_l}$, where $\rho_{\mathcal{E}_l}$ is the reflectivity of the element.

B. Impulse Response Calculations

The IR radiation incident upon a receiver $\mathcal{R}_j$ will be the result of the radiation emitted from a source $\mathcal{S}_i$ that has propagated directly through an unobstructed LOS path, and/or from the radiation that has undergone a finite number, k, reflections off the surfaces within the environment. It is also known [24], [25] that, for an intensity modulation, direct detection (IM/DD) channel, where the movement of transmitters, receivers or objects in the room is slow compared to the bit rate of the system, no multipath fading occurs, and, as such, can be deemed an LTI channel. The impulse response $h(t; \mathcal{S}_i, \mathcal{R}_j)$ is given by [25], [26]

$$h(t; \mathcal{S}_i, \mathcal{R}_j) = \sum_{k=0}^{k} h^k(t; \mathcal{S}_i, \mathcal{R}_j) \quad (2)$$

where $h^k(t; \mathcal{S}_i, \mathcal{R}_j)$ is the impulse response of the system for radiation undergoing k reflections between $\mathcal{S}_i$ and $\mathcal{R}_j$.

To determine the impulse response, we assume our source $\mathcal{S}_i$ emits a unit impulse at $t = 0$, i.e setting $P_{\mathcal{S}_i} = 1\text{W}$, then
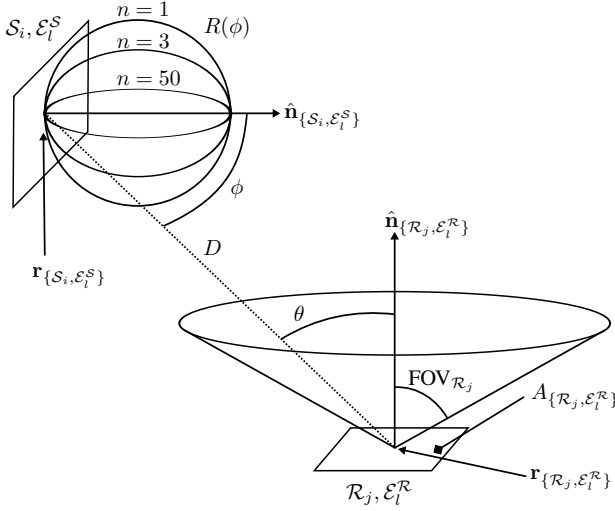
Fig. 1. Source, receiver and reflector geometry, adapted from [25]

the LOS ($k = 0$) impulse response is given by the scaled and delayed Dirac delta function

$$h^0(t; \mathcal{S}_i, \mathcal{R}_j) \approx R(\phi_{ij}) \frac{\cos(\theta_{ij}) A_{\mathcal{R}j}}{D_{ij}} V(\frac{\theta_{ij}}{\text{FOV}_{\mathcal{R}j}}) \delta(t - \frac{D_{ij}}{c})$$
(3)

Where, referring to figure 1, $D_{ij} = ||\mathbf{r}_{\mathcal{S}_i} - \mathbf{r}_{\mathcal{R}_j}||$ is the distance between source and receiver, c is the speed of light. ϕ_{ij} and θ_{ij} are the angles between $\hat{\mathbf{n}}_{\mathcal{S}_i}$ and $(\mathbf{r}_{\mathcal{R}_j} - \mathbf{r}_{\mathcal{S}_i})$ and between $\hat{\mathbf{n}}_{\mathcal{R}_j}$ and $(\mathbf{r}_{\mathcal{S}_i} - \mathbf{r}_{\mathcal{R}_j})$ respectively. $V(x)$ represents the the visibility function, where $V(x) = 1$ for $|x| \leq 1$, and $V(x) = 0$ otherwise.

For radiation undergoing $k > 0$ bounces, the impulse response is given by

$$h^k(t; \mathcal{S}_i, \mathcal{R}_j) = \sum_{l=1}^{L} h^{(k-1)}(t; \mathcal{S}_i, \mathcal{E}_l^{\mathcal{R}}) * h^0(t; \mathcal{E}_l^{\mathcal{S}}, \mathcal{R}_j)$$
(4)

Where $*$ denotes convolution, and the $k - 1$ impulse response $h^{(k-1)}(t; \mathcal{S}_i, \mathcal{E}_l^{\mathcal{R}})$ can be found iteratively [26] from

$$h^k(t; \mathcal{S}_i, \mathcal{E}_l^{\mathcal{R}}) = \sum_{l=1}^{L} h^{(k-1)}(t; \mathcal{S}_i, \mathcal{E}_l^{\mathcal{R}}) * h^0(t; \mathcal{E}_l^{\mathcal{S}}, \mathcal{E}_l^{\mathcal{R}})$$
(5)

Where all the zero order ($k = 0$), responses in (4) and (5) are found by careful substitution of the variables in (3). The computational time required for calculation of the impulse response using this iterative method is proportional to k^2 [27], and we will firstly limit ourselves to the a third order impulse response ($k = 3$), and secondly change the segmentation resolution of the environment for each reflection, setting $\Delta A_1 = 20$, $\Delta A_2 = 6$ and $\Delta A_3 = 2$. It should also be noted that the resultant impulse response in (2) will result in the finite sum of scaled delta functions which need to undergo temporal smoothing by subdividing time into bins of width Δt, and summing the total power in each bin [25]. For this work, we assume a single time bin width of $\Delta t = 0.1$ns.

III. THE CHANNEL MODEL

A. Scaling Factors

For a nondirected IR channel employing IM/DD, a source $\mathcal{S}_i$ which emits an instantaneous optical power $X_i(t)$, will produce a instantaneous photocurrent $Y_{ij}(t)$ at receiver $\mathcal{R}_j$ with photodiode responsivity r_j, in the presence of an additive, white Gaussian shot noise $N_j(t)$, and can modelled as the linear baseband system given by [28]

$$Y_{ij}(t) = r_j X_i(t) * h(t; \mathcal{S}_i, \mathcal{R}_j) + N_j(t)$$
(6)

Where $h(t; \mathcal{S}_i, \mathcal{R}_j)$ is the impulse response given by (2), and is fixed for a given system configuration of $\mathcal{S}_i$ and $\mathcal{R}_j$.

Assuming that all I sources $\mathcal{S}_i$ emit an identical signal waveform, such that $X_1(t) = X_2(t) = \ldots = X_I(t)$, but whose magnitude is individually scaled by a factor a_i, the instantaneous photocurrent generated at a given receiver $Y_j(t)$ is simply the summation of (6) for all sources:-

$$Y_j(t) = \sum_{i=1}^{I} (r_j a_i X_i(t) * h(t; \mathcal{S}_i, \mathcal{R}_j)) + N_j(t)$$
(7)

Furthermore, as we are only concerned with a single receiver design, the photodiode responsivity r_j is constant for each receiver or receiver location, such that there may exist a set of I scaling factors a_i, that can be applied to the I identical signal waveforms $X_i(t)$, that will allow for the J receivers, to attain the same or very similar instantaneous photocurrents

$$Y_1(t) \approx Y_2(t) \approx \ldots \approx Y_J(t)$$
(8)

Knowing that the channel is linear we can rewrite (7) as

$$Y_j(t) = \sum_{i=1}^{I} (r_j X_i(t) * a_i h(t; \mathcal{S}_i, \mathcal{R}_j)) + N_j(t)$$
(9)

Such that we can solve (8) by solving

$$\sum_{i=1}^{I} a_i h(t; \mathcal{S}_i, \mathcal{R}_1) \approx \sum_{i=1}^{I} a_i h(t; \mathcal{S}_i, \mathcal{R}_2) \approx \ldots$$
$$\ldots \approx \sum_{i=1}^{I} a_i h(t; \mathcal{S}_i, \mathcal{R}_J)$$
(10)

By inspection of equations (7) to (10), it can be seen that a solution may require some scaling factors of ≤ 1, lowering the total received power, compared to if all sources were the same. Furthermore solving (8) for different environments, will yield non-identical sets of scaling factors implying the magnitude of received power, although equal at all locations within, will be different.

Under IEC825 regulations [29], the maximum acceptable exposure limit (AEL), is based upon variable factors such as wavelength, exposure duration, pulse characteristics and image size [30]. Two source factors in particular, diameter and divergence, can be increased allowing for a higher AEL [4]. A 2-D VCSEL/RCLED array will emit multiple low divergence beams upon the ceiling. The divergence of the emitted beams, coupled with the Lambertian reflection characteristics of the ceiling, and the fact that the human eye cannot subtend all the resultant diffusion spots simultaneously, increases the AEL

compared to a conventional point source. The same logic can also be applied when using multiple LEDs, as they have a larger diameter than a point source. Whilst the GA will adapt the power of each diffusion spot, the system must still be within the AEL at the worst case of all spots at maximum.

Drawing parallels with the IEEE 802.11a WiFi physical layer specification, that incorporates multi-rate transmission of up to 54Mbit/s [31], and recent work on rate-adaptive transmission [32] in the IR domain, if it is found that several environments have different received powers the following method can be applied. Firstly by normalising the I scaling factors, the equality result of (8) is independent of receiver power magnitude, and secondly for different environments we can adjust for example, the pulse characteristic, in order to increase or decrease the received power to make the power distributions equal. This then allows for the same optimal receiver design to be used in different environments, albeit under the compromise of variable data rates in the same manner as most other variable data rate systems.

To illustrate the final problem simplification we have applied, consider for example an environment such as configuration A in [25], with dimensions $x = 5\text{m}, y = 5\text{m}, z = 3\text{m}$. In calculating a third order reflection impulse response ($k = 3$), the longest time of flight for the radiation to travel is $t = (4(5^2 + 5^2 + 3^2)^{0.5})/c \approx 102.4\text{ns}$, when it undergoes a path reflecting off the opposite corners of the room. Using an impulse response bin width $\Delta t = 0.1\text{ns}$, would produce 1024 samples for each impulse response train, for every combination of I sources and J receivers in (10).

In the general case, proposing a GA that can solve (10) for the possibly infinite number of source and transmitter configurations would prove to be too unwieldy. By replacing the need to evaluate each bin of the impulse response train, with the need to find only the scaling factor solution for the time integral or the DC value of the frequency response $H(0; \mathcal{S}_i, \mathcal{R}_j) = \int_{-\infty}^{\infty} h(t; \mathcal{S}_i, \mathcal{R}_j)dt$, equation (10) reduces to

$$\sum_{i=1}^{I} a_i H(0; \mathcal{S}_i, \mathcal{R}_1) \approx \sum_{i=1}^{I} a_i H(0; \mathcal{S}_i, \mathcal{R}_2) \approx \dots$$
$$\dots \approx \sum_{i=1}^{I} a_i H(0; \mathcal{S}_i, \mathcal{R}_J) \quad (11)$$

The power distribution optimisation should not be achieved at the expense of bandwidth and rms delay spread. As (11) only quantifies the total power received, not when the power was received we will feed back the solution into the original system model to quantify our worst case bandwidth and rms delay spread, defined as the smallest and largest values at any location within the room respectively. The rms delay spread can be found from the original impulse response using [33]

$$\sigma = \sqrt{\frac{\int_{-\infty}^{\infty} (t - \omega)^2 h^2(t)dt}{\int_{-\infty}^{\infty} h^2(t)dt}} \quad (12)$$

Where ω is defined as:

$$\omega = \frac{\int_{-\infty}^{\infty} t h^2(t)dt}{\int_{-\infty}^{\infty} h^2(t)} \quad (13)$$

IV. THE GENETIC ALGORITHM

GAs should not be considered off-the-peg, ready to use algorithms, but rather a general framework that needs to be tailored to a specific problem [34]. Below we describe our methodology and justifications for decisions made in adapting the representation, fitness function, selection, recombination and mutation routines found in a so-called *canonical* GA.

A. Representation

The genotype represents all the information stored in the chromosome and allows us to describe an individual at the level of the genes. Our aim is to find a set of scaling factors that can be used to solve (11), such that if we allow $a_i \forall i \in \{1, \dots, I\}$ to take on a value in the set $\{0, 0.01, \dots, 1\}$, we can define our genotypic search space $\Phi_g = \{0, 0.01, \dots, 1\}^I$, which will provide $|\Phi_g| = 101^I$ possible solutions [35]. We further define a population $\Psi(t)$ at time t, of μ chromosomes $\mathbf{a}_\nu = (a_1, \dots, a_I) \in \Phi_g, \forall \nu \in \{1, \dots, \mu\}$ which provide our basic representation of a possible solution in a form that can be operated on by the GA. The initial population of chromosomes is formed by a uniform pseudo random number generator capable of only generating numbers in the set $\{0, 0.01, \dots, 1\}$, such that the larger the population the better the chance of an initialisation with a uniform distribution of possible solution values. However, this would also require a larger memory overhead on the hardware implementation, and so we need to find the smallest population size that will not adversely affect the GAs performance when some ratios are not initialised, and subsequently cannot be evaluated as a possible solution. We will therefore evaluate population sizes $\mu = \{50, 100, 200\}$.

We are also going to investigate what is known as chromosome epistasis, which refers to a problem-dependent condition in the genotype structure where genes are highly interdependent, such that a good solution may only be found when the value of the genes occur in a particular pattern [36]. Consider for example a system with $I = 16$, such that our chromosome will contain 16 scaling factors as in figure 2(a), which translate to the sources on the ceiling in two ways depending upon how we define our genotype structure $\mathcal{G}$. Implementing a wrap-around, ($\mathcal{G} = \text{WA}$) structure the scaling factors translate to their respective sources as in figure 2(b), and it can be seen that scaling factors a_4 and a_5, a_8 and a_9 etc. are physically far apart in application, but adjacent in the chromosome. Alternatively, a concertina ($\mathcal{G} = \text{CON}$) structure as in figure 2(c), now shows this problem is alleviated, but other scaling factors, such as a_1 and a_8, are now physically close, whilst further apart in the chromosome. We will test for this condition by applying identical GAs for each genotype structure.

B. The Fitness Function

Whereas the genotype describes an individual on the level of the genes, the phenotype describes its outward appearance, and it is this phenotypic appearance that determines an individuals success in life. The GAs genetic operators, such as recombination and mutation, work on the level of the genes, but offspring of parents do not inherit the phenotypic properties,
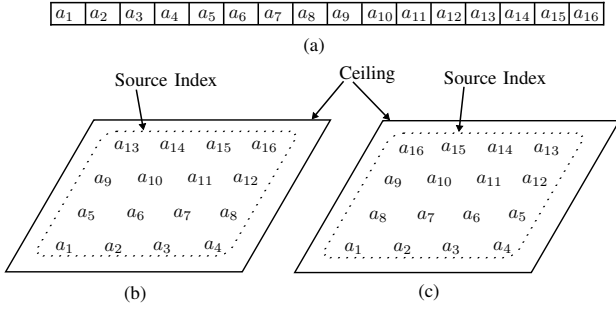
Fig. 2. Chromosome epistasis. (a) Chromosome structure. (b) Wrap around genotype structure. (c) Concertina genotype structure.

only the genotypic properties which still require evaluation at the level of the phenotype [35]. This evaluation is commonly known as the fitness, or objective function, F, which, for the results presented here, is given by

$$F(\mathbf{a}_\nu) = 100 - \left(100 \left(\frac{\max H(0; \mathbf{a}_\nu) - \min H(0; \mathbf{a}_\nu)}{\max H(0; \mathbf{a}_\nu)} \right) \right) \tag{14}$$

Where $\max H(0; \mathbf{a}_\nu)$ and $\min H(0; \mathbf{a}_\nu)$ are the maximum and minimum DC frequency responses at any receiver in the environment after application of the scaling factors $\mathbf{a}_\nu$ to the source powers, respectively. It can be seen that we are measuring the percentage change or deviation from the peak power in the room, for an individual $\mathbf{a}_\nu$, whose source scaling factors will produce a perfectly uniform power distribution within the room and will have a fitness of 100%. Furthermore, we can define our global maximum optimal solution $\hat{\mathbf{a}}_\nu$ to be

$$\hat{\mathbf{a}}_\nu = \max_{\mathbf{a}_\nu \in \Phi_g} F(\mathbf{a}_\nu) \tag{15}$$

In general the choice of a fitness function is one of the more difficult steps in constructing an optimal GA, as the decision is not only problem specific but inherently dependent upon the genotype representation used. Therefore whilst we have applied, for the reasons given in section III-A, a normalised fitness function, based upon a maximum and minimum values of the power deviation, it would be theoretically feasible to use any of a number of mathematical measures, such as mean deviation, provided it fits within the users overall GA structure.

C. Selection

The primary objective of the selection operator is to emphasise the fitter solutions, with either an explorative or exploitative bias, such that their genotypic information is passed onto the next generation [37]. We implement three selection routines in this work namely, roulette, stochastic uniform sampling (SUS) [38] and tournament selection.

The roulette and SUS selection schemes assign a probability of selection proportional to an individual's relative fitness within the population, such that an individual's probability of selection, p_ν^{prop}, is given by

$$p_\nu^{\text{prop}} = \frac{F(a_\nu)}{\sum_{\nu=1}^{\mu} F(a_\nu)} \tag{16}$$

These probabilities are then contiguously mapped onto a wheel, such that $\sum_{\nu=1}^{\mu} p_\nu^{\text{prop}} = 1$. A uniform random number is then generated in the interval $[0, 1]$, and the individuals whose cumulative probability within the population that spans the number is chosen. The process is repeated μ times, until a new population has been selected. The roulette wheel is unbiased but suffers from a possible infinite spread, in that statistically any member of the population with $p_\nu^{\text{prop}} > 0$ can be chosen μ times for the next generation. SUS overcomes this by generating μ uniformly spaced numbers in the range $[0, 1]$, and applying a single randomly generated offset value, that moves the position of the numbers such that each individual is still selected based upon its cumulative probability position relative to others in the population. It thus maintains zero bias, but now it is not possible for a given individual to be chosen beyond its expected number [38].

Tournament selection is carried out by first ranking all members in the population $\Psi(t) = \{\mathbf{a}_1, \ldots, \mathbf{a}_\mu\}$ by their absolute fitness in the population $F(\mathbf{a}_\nu)$, where $\mathbf{a}_1$ is the fittest, and $\mathbf{a}_\mu$ is the least. Then, by randomly selecting q members, we choose the best for the next generation. The probability of a member $\mathbf{a}_\nu$ being selected is given by [37]

$$p_\nu^{\text{torn}} = \frac{1}{\mu^q} \left((\mu - \nu + 1)^q - (\mu - \nu)^q \right) \tag{17}$$

Increasing the size of the tournament q increases the selective pressure, giving fitter members of the population a higher probability of selection. With our chosen population sizes, we can expect that, as we are going to implement tournament selection with $q = 2$ and $q = 3$, we will lose approximately 40% and 50% of the genetic material, respectively, through the selection process alone [39]. This gives rise to a very exploitative algorithm, but it looses genetic diversity and risks finding a non optimal solution. However, as tournament selection does not require proportional fitness assignments as in (16), the algorithm operates faster. As previously mentioned the size of the population will dictate hardware memory requirements, but for a mobile applications the speed of the algorithm equates to adaptive latency, vital to usability of the system for both receivers within, entering or leaving the room.

D. Reproduction

Crossover imitates the principles of natural reproduction, and is applied with a probability of ρ_c to randomly selected individuals chosen by the selection routine. Its purpose is to form new individuals for the next generation which have some parts of the genotypic information as their parents. For this work we apply a single point $m = 1$ and double point $m = 2$ crossover. In a single point crossover, a random crossover point in the range $\{1, \ldots, I - 1\}$ is chosen, and two new individuals are formed by swapping the substrings about that point. For a double point crossover, a similar method is applied, but by generating two unique random numbers in the range $\{1, \ldots, I - 1\}$, and sorting into ascending order, followed by exchanging substrings between successive cross over points. For this work we maintain $\rho_c = 0.7$.

E. Mutation

Mutation was originally developed as a background operator [34], able to introduce new genetic material into the search routine such that the probability of evaluating a string in Φ_g will never be zero. Thus it would still be possible to recover good genetic information that may have been lost through selection [35]. Unlike the crossover operator, mutation is seen as a local search method, because it can only modify elements of an individual, perturbing its genetic information in a much smaller way than crossover, which allows the combining of genotypic information from different parents. As we are going to evaluate different selection routines, we will apply the mutation operator to each gene in each individual with varying probabilities $\rho_m = \{0, 0.05, 0.1, 0.2\}$, such that when a random number is generated that is less than the chosen probability, we replace that gene with a new randomly-generated value in the set $\{0, 0.01, \ldots, 1\}$. We will attempt to find the highest possible value aiding in the search, but not too high that we encounter what is know as mutation interference defined as when the mutation rate is so high that solutions are so frequently or drastically mutated that the algorithm never manages to explore any region of the search space thoroughly as good solutions, rather than being formed by mutation, are rapidly destroyed [36].

F. Feedback, Termination and Repeatability

Some feedback loop must exist that passes back information regarding the effectiveness of a solution at each generation. Presently the simulation will simply return the DC gain at each receiver location to the fitness function. In a practical system we envisage two methods. Firstly that the receiver, or more precisely transceiver, returns the DC gain or SNR using a supervisory audio tone similar to GSM techniques, or secondly if this optimisation process has been simulated on many scenarios, and the best and worst case powers are known, the transceiver could simply return a 'too high' or 'too low' command, informing the transmitter some change should be made to the ratios. Either method could be applied as and when needed, or within some predefined protocol space, and would be suitable when one or many receivers are present. Moreover, both methods are applicable when users enter or leave the room, since in theory, they too have the same receiver design that requires the same power distribution to operate.

In general, a GA is run over many generations until the algorithm converges or the result has satisfied some defined solution criteria. As we were unaware of what the minimum power deviation for a given room will be, we decided upon 5000 generations, as this was a reasonable compromise between computational effort, and allowing the algorithm to search for better solutions. As will be shown in section V, all GAs (that would converge) converged within this time frame.

Due to the stochastic nature of the GA, for each simulation the results were inevitably slightly different, meaning that to allow presentation of results that are both representative of the GAs performance and repeatable for the reader to follow, we conducted each simulation 30 times, such that each
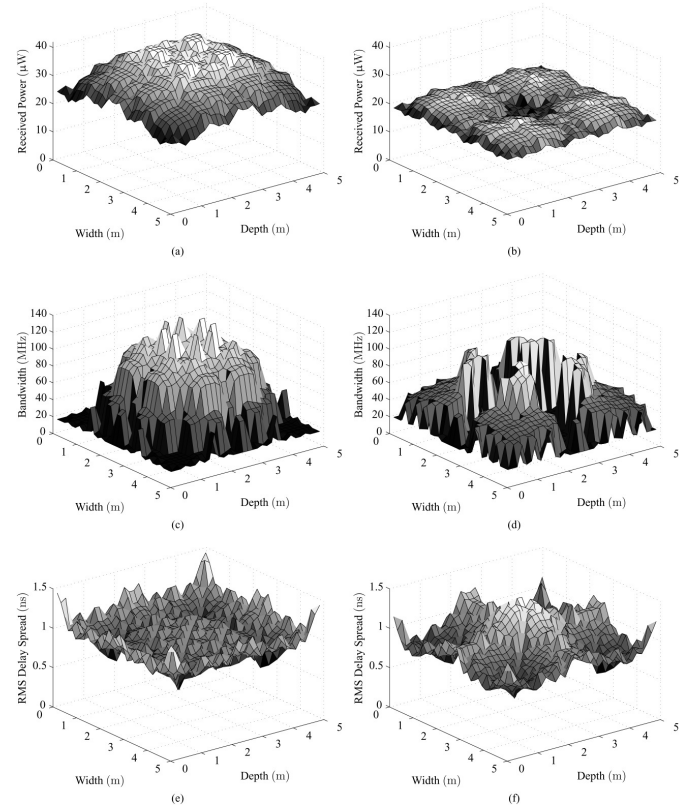

Fig. 3. Empty algorithm test room power, bandwidth and rms delay spread distributions. (a) Non optimised power distribution. (b) Optimised power distribution. (c) Non optimised bandwidth distribution. (d) Optimised bandwidth distribution. (e) Non optimised rms delay spread distribution. (f) Optimised rms delay spread distribution.

performance value presented within section V is the average and the associated standard deviation after the 30 retrials.

V. RESULTS

A. Algorithmic Properties

To begin to understand how the GA optimisation would perform, we began by simulating the impulse response of the empty algorithm test room similar to configuration A in [25], with width $x = 5$m, depth $y = 5$m and height $z = 3$m, each wall and ceiling having a reflectivity $\rho = 0.8$, and the floor having a reflectivity of $\rho = 0.3$. 16 sources were uniformly distributed over the ceiling, orientated towards the floor, with a Lambertian radiation profile $n = 1$. At a height of $z = 1$m, 1024 receivers, with a $FOV_{\mathcal{R}_j} = 45°$ and area $A_{\mathcal{R}_j} = 0.0001$m^2 were orientated towards the ceiling. The power, bandwidth and rms delay spread distribution can be seen in figures 3(a), 3(c) and 3(e), where a peak and minimum power of 41μW and 22μW, respectively, can be observed, equating to 19μW, or 46% power deviation from the peak. The bandwidth varies between 14MHz and 134MHz whilst the rms delay spread ranges between 0.6ns and 1.5ns.

Considering our primary concern of how well a certain set of GA parameters can reduce the deviation of received power relative to peak power, such that the best GA is the one that produces the lowest deviation (LwD). Table I presents these

TABLE I
THE 12 BEST ALGORITHMS

Algorithm	Selection Method	μ	ρ_m	m	$\mathcal{G}$	LwD (St.D)
1	Roulette	50	0.1	2	CON	36(1.8)
2	Roulette	100	0.1	2	WA	34(1.0)
3	Roulette	200	0.05	2	WA	32(0.9)
4	SUS	50	0.05	2	CON	31(0.8)
5	SUS	100	0.05	1	CON	31(0.5)
6	SUS	200	0.05	2	CON	30(0.3)
7	Tournament (2)	50	0.2	2	CON	33(1.3)
8	Tournament (2)	100	0.2	2	WA	32(1.0)
9	Tournament (2)	200	0.2	2	CON	31(1.0)
10	Tournament (3)	50	0.2	2	CON	33(1.2)
11	Tournament (3)	100	0.1	2	CON	32(1.1)
12	Tournament (3)	200	0.2	2	CON	32(0.8)

Fig. 4. Convergence curves for algorithms $2, 6$ and 11. Insert depicts the 16 normalised ratios for the respective spot positions provided by the last generation of algorithm 6.

best parameters from section IV for a given selection scheme and population size. The LwD from peak power is related to the fitness function in (14) by LwD $= 100 - F(\mathbf{a}_\nu)$, thus the LwD values are measured as a %.

The most effective optimisation for this scenario came from applying algorithm 6, as it found the LwD of power and with the lowest standard deviation, implying a high degree of repeatability giving us confidence in its ability to constantly return the best solution. Applying the source scaling factors provided by algorithm 6, as in figures 3(b), 3(d), and 3(f), the received power now deviated 32% between 17µW and 25µW. This improvement in power distribution also led to a change in bandwidth and rms delay spread distribution. The bandwidth now varied between 14MHz to 110MHz, which, while it showed a 24MHz reduction in the peak bandwidth, our worst case performance criteria, the lowest bandwidth remained the same. The rms delay spread ranged from 0.5ns to 1.4ns, little changed from the baseline case.

In terms of how each selection routine performed relative to each other, figure 4 shows the convergence curves of the best individual within the population for algorithms $2, 6$ and 11 of table I at each generation. The curves shown are typical for a given selection scheme, with only the point of convergence changing by varying the parameters such as mutation rate, number of crossover points and genotype structure. The insert to figure 4 details the normalised ratios found in the final generation of algorithm 6 in their respective positions upon the ceiling. These ratios can be used to produce the results of figures 3(b), 3(d), and 3(f). An interesting result of these ratios and their positions is the apparent symmetry of the ratios, around the center of the ceiling. Whereas the work described in this paper, relies on fixed spot position and varying intensities, other work has been presented [40], [41], that varies spot position at fixed intensities. The elegance of applying the GA does not rule out reproducing, albeit not perfectly due to spacing of our uniform spot distribution, any of these established spot patterns, such as uniform, diamond or line-strip [15], by simply setting some of the ratios to be 0 and some to 1. However the GA ratios are not restricted to any spot pattern and so, as will be shown in section V-C, could prove to be more adaptable in the event of user movement, or alternative environments.

SUS selection routines performed the most predictably and with the best overall results. The slow and gradual convergence to a solution was always achievable, even at higher mutation
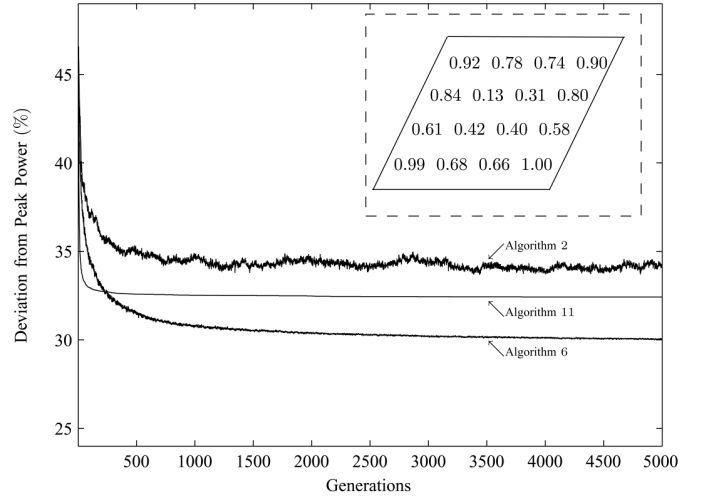
rates ($\rho_m = 0.1$), although best performances were always found when $\rho_m = 0.05$. They also performed better with the concertina genotypic structure ($\mathcal{G} = \text{CON}$), achieving around $1 - 2\%$ improvement over a routine with identical parameters and a wrap around structure ($\mathcal{G} = \text{WA}$). The use of a double point cross over ($m = 2$) improved the standard deviation, that is, its repeatability, but seemed to have little effect on the ability to converge to better solutions. Finally the highest population size ($\mu = 200$), appeared to be preferential in gaining lower power deviation, compared to setting $\mu = 100$.

Tournament selection, with either 2 or 3 tournament candidates, tended to quickly but sub-optimally converge. As can be seen from figure 4, beyond 500 generations, the selection routine will not allow for new solutions to be considered, even when using a high mutation rate ($\rho_m = 0.2$) in order to overcome the predicted 50% loss of diversity encountered from the *greedy* nature of the selection scheme. This high level of genotypic information removal also meant that performance was very similar when $\mu = 100$ and $\mu = 200$ for a given set of parameters, as regardless of the information formed upon initialisation, the algorithm had no time to thoroughly search the solution space. Very little dependence was shown upon the number of crossover points used, but generally produced better results using the concertina genotype structure ($\mathcal{G} = \text{CON}$).

Roulette selection was by far the worst performing of all tested, showing no consistency or pattern towards either how well an algorithm would perform, or to why a performance level was achieved. Variation of one parameter resulted in contradictory behaviour for any other developed parameter relations. Figure 4 illustrates the chaotic nature of the convergence curve for algorithm 2, seemingly losing good genetic information from one generation to the next.

B. Source Number and FOV Variations

Continuing with the same room, we now vary the number of sources from 9 to 25, and the receiver's FOV between $10°$ and $85°$, to draw out more optimisation relationships. As the GA

TABLE II
EMPTY TEST ROOM POWER OPTIMISATION USING ALGORITHM 6 FOR
VARYING NUMBER OF SOURCES AND RECEIVER FOV'S

| FOV | No. Spots | | | | | |
| | 9 | | 16 | | 25 | |
	NOD	OLD(St.D)	NOD	OLD (St.D)	NOD	OLD (St.D)
10°	98	98(0.0)	96	96(0.0)	94	94(0.0)
15°	95	95(0.0)	92	91(0.0)	92	92(0.0)
25°	90	90(0.0)	54	54(0.2)	60	59(0.4)
35°	62	56(0.2)	61	49(0.3)	66	42(1.4)
45°	54	36(0.4)	46	30(0.3)	45	29(0.3)
55°	45	25(0.4)	46	25(0.3)	44	23(0.4)
65°	44	30(0.2)	45	29(0.4)	45	27(0.3)
75°	42	30(0.2)	42	26(0.4)	42	25(0.3)
85°	42	30(0.2)	42	27(0.3)	42	26(0.3)

technique will add some complexity to the transmitter driver electronics, we resisted the urge to go beyond 25 sources, so as still to keep the system cost effective. Table II presents the results for the optimised lowest deviation (OLD) from peak power as a % and the standard deviation of the multiple runs using algorithm 6, compared to the non optimised deviation from peak power (NOD)(%).

For a receiver with a $FOV_{\mathcal{R}_j} < 35°$, virtually no optimisation can be achieved. This is down to the fact that at these small FOV's, the receiver does not detect much power from the multiple reflections off the surfaces of the environment, as for example figures 5(a) and 5(b) which show the before and after optimisation of a receiver with a $FOV_{\mathcal{R}_j} = 15°$ under 16 spots. In contrast to this is a receiver with a slightly higher $FOV_{\mathcal{R}_j} = 35°$ under 25 spots, which is the configuration that can be optimised the most, the power being reduced from a deviation of 66%, to 42%, as in figures 5(c) and 5(d). Using a receiver with a $FOV_{\mathcal{R}_j} = 55°$ under 25 spots provides the configuration with the lowest optimised change in power from peak at only 23%, which can be seen in 5(e) and 5(f).

As in previous results, using the GA to reduce the deviation of the received power has negligible effects on the bandwidth and RMS delay spread. As shown in figure 6, for the lower FOV's, where no optimisation is achieved, both the optimised and non optimised, minimum bandwidth and largest rms delay spread remain the same. For higher FOV's, the maximum rms delay spread is relatively unchanged, and the bandwidth has been reduced by around 2MHz at some FOV's.

One affirmation to make with the bandwidth results of figure 6, is that they show our performance criteria of lowest possible bandwidth at any receiver position within the room. Whilst it can be observed that the bandwidth increases slightly with increasing FOV, a concept that may seem contrary to traditional thought, these worst case results are found near the walls of the room, as can be seen in figure 3(c-d). At these positions, a receiver and ceiling diffusion spot, are 8cm and at least 50cm from the wall, respectively. This means that at the lower FOV's, there is no direct LOS link present, consequently all incident radiation is a result of multiple reflections, lowering the bandwidth. As the FOV increases, more LOS links are formed, and the power from the LOS links is larger, relative to the power from reflections, increasing bandwidth. Finally, at the very large FOV's, the worst case bandwidth reduces slightly as the magnitude of power from reflections increase relative to that from the LOS links.
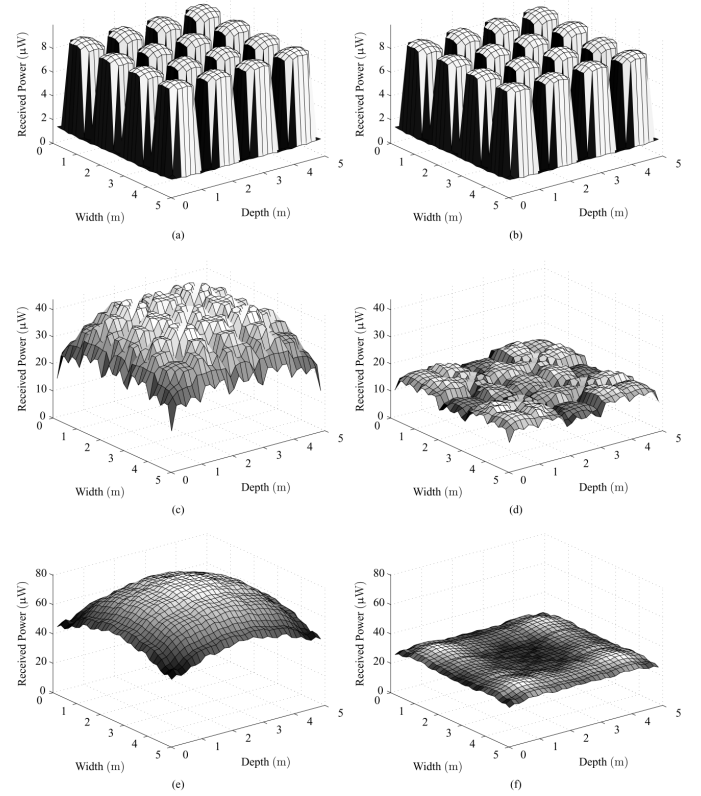

Fig. 5. Empty test room power optimisation using algorithm 6 for varying number of sources and receiver FOV's. (a) Non optimised, $FOV_{\mathcal{R}_j} = 15°$, 16 spots. (b) Optimised, $FOV_{\mathcal{R}_j} = 15°$, 16 spots. (c) Non optimised, $FOV_{\mathcal{R}_j} = 35°$, 25 spots. (d) Optimised, $FOV_{\mathcal{R}_j} = 35°$, 25 spots. (e) Non optimised, $FOV_{\mathcal{R}_j} = 55°$, 25 spots. (f) Optimised, $FOV_{\mathcal{R}_j} = 55°$, 25 spots.

C. Moving Objects

Using a simple ray tracing intersection algorithm [42], an object, representing a person with a height $z = 1.8m$, shoulder to shoulder width $x = 0.7m$, front to back depth $y = 0.4m$ and reflectivity $\rho = 0.3$ [26], was modelled undertaking two different movement patterns as shown in figure 7. To quantify the GAs ability to work in real world scenarios, we implemented movement pattern 1 in our established environment, and movement pattern 2 in an environment of the same dimensions, but reducing the reflectivity of the ceiling to $\rho = 0.75$, north wall to $\rho = 0.7$ and east wall to $\rho = 0.6$. We reiterate that although the person is moving, they are not moving fast enough to break the multipath fading criteria set out in section III. Based on the results of section V-B, we implemented a system with 25 ceiling spots, with a receiver $FOV_{\mathcal{R}_j} = 55°$, such that we are using the configuration we thought could attain the lowest possible power deviation.

Given that our receiver locations are in fixed uniformly distributed positions, and that objects are now placed within the environments, the fitness function may not correctly handle a receiver *inside* an object, as the incident power will be zero. To accommodate this we place an exclusion zone, where no information is passed back to the GA, around the person of 10cm which is roughly the minimum distance that a portable receiver, such as a mobile phone could be placed next the body.
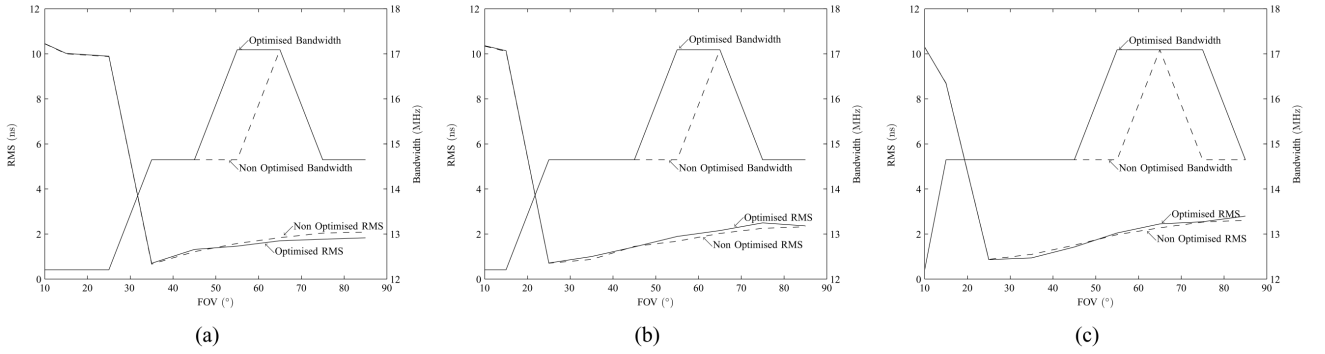
Fig. 6. Empty test room bandwidth and rms delay spread optimisation using algorithm 6 for varying number of sources and receiver FOV's. (a) 9 spots. (b) 16 spots. (c) 25 spots.
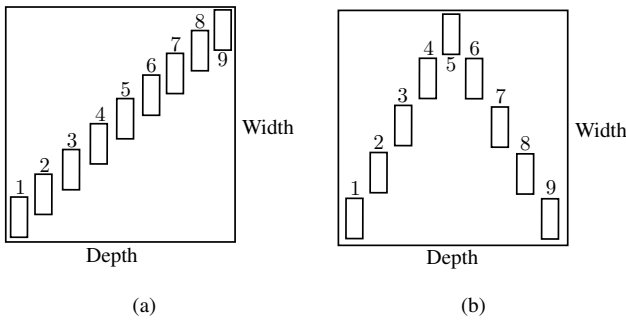

Fig. 7. The nine movement positions. (a) Pattern 1. (b) Pattern 2.

This issue is a limitation of the GA, not the channel response simulation, or intersection algorithm which handled receiver's blocked by objects correctly. We also tested algorithm 11 in table I, as it uses a tournament 3 selection routine. It was shown to be capable of finding solutions to within a few % of algorithm 6 using a lower population size and without the need to compute proportional fitnesses, therefore allowing simpler transmitter hardware implementation, or just as importantly, exhibit a lower adaptation latency.

Considering an empty environment 1, the deviation from peak power is just under 45%, as shown in figure 8(a), and optimising using algorithm 6 and algorithm 11, reduces the deviation by around 21% and 18% respectively. Environment 2 when empty, as shown in figure 8(b), has a slightly higher power deviation at 52% with algorithm 6 and algorithm 11 reducing the power deviation by 26% and 24% respectively. Similar to the results of table I, algorithm 6 outperforms algorithm 11 by a few percent, highlighting the consistency in the GAs performance characteristics when scaled to different environments. When the person is moving in either room, they perturb the power distribution, as they themselves become reflectors, up to an influence of 19% change. We stress that this power deviation is a measure of the difference between maximum and minimum over all locations within the room, not just the receiver in use by the moving person, such that it is possible that all users are affected by the movement.

Furthermore from figure 8, both algorithms, in both environments, when exposed to different user movement patterns,

manage to track the movement, and not only maintain an optimised power distribution below the original empty room, but also now keep the effect of the moving person down to a perturbation of 12% for environment 1 and 18% for environment 2. Position 9 of environment 2 may show the first signs of the what is still a technique limited to what is physically achievable. While the algorithm has managed to reduce the deviation from peak power by 25%, it happened to be at a position in the room where the influence of the person was such that they had a very large effect on the power distribution, influencing the largest change out of all the positions in both rooms.

Figure 9 shows the relationship between the non-optimised bandwidth (NOB), rms delay spread (NOrms) and optimised bandwidth (OB) and rms delay spread (Orms) for both environments while empty (/E), and with movement (/M). The results reinforce further that, while the GA is capable of optimising the received power around the room, it will not alter the worst case bandwidth or rms delay spread by more than $3\,\mathrm{MHz}$, and $< 0.3\,\mathrm{ns}$, respectively, which may be an acceptable compromise for the purposes of an OW system, given the advantages this technique might provide for a single optimal hardware solution to multiple dynamic environments.

The final question based on these results is what FOV a designer may choose to use? For the scenarios simulated here, a receiver design would be based upon a $\mathrm{FOV}_{\mathcal{R}_j} = 55°$ as the GA is most effective, for our chosen metric in (14), at this FOV. However the GA method proposed, although shown to be viable and advantageous in its application, is only one stage in the design process. A specific product deployment scenario may have constraints, such as higher than average ambient light conditions, that excludes the use of a $\mathrm{FOV}_{\mathcal{R}_j} = 55°$. Ideally the simulations would need to be completed in rooms encompassing the end users, their movement patterns, and the commonly found materials in the systems targeted deployment environment. The final FOV decision would then be based upon the results generated in conjunction with any ancillary considerations.

VI. CONCLUSION

This paper has demonstrated the novel approach of using a GA controlled MSD transmitter, capable of optimising
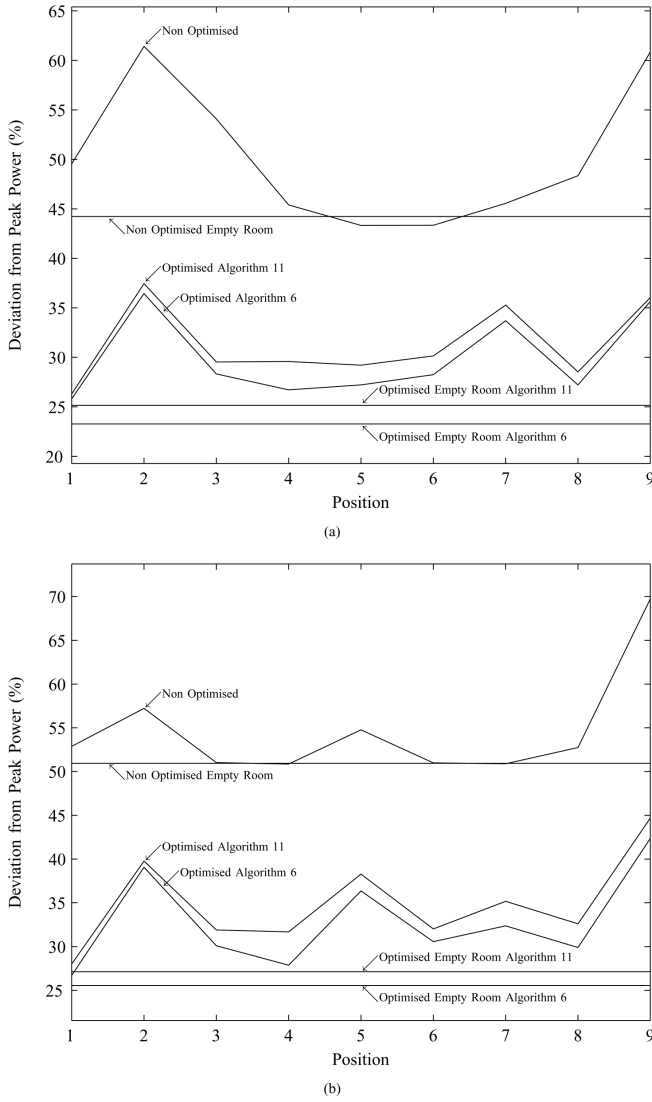
Fig. 8. Power distribution in two dynamic environments. (a) Environment 1, movement pattern 1. (b) Environment 2, movement pattern 2.
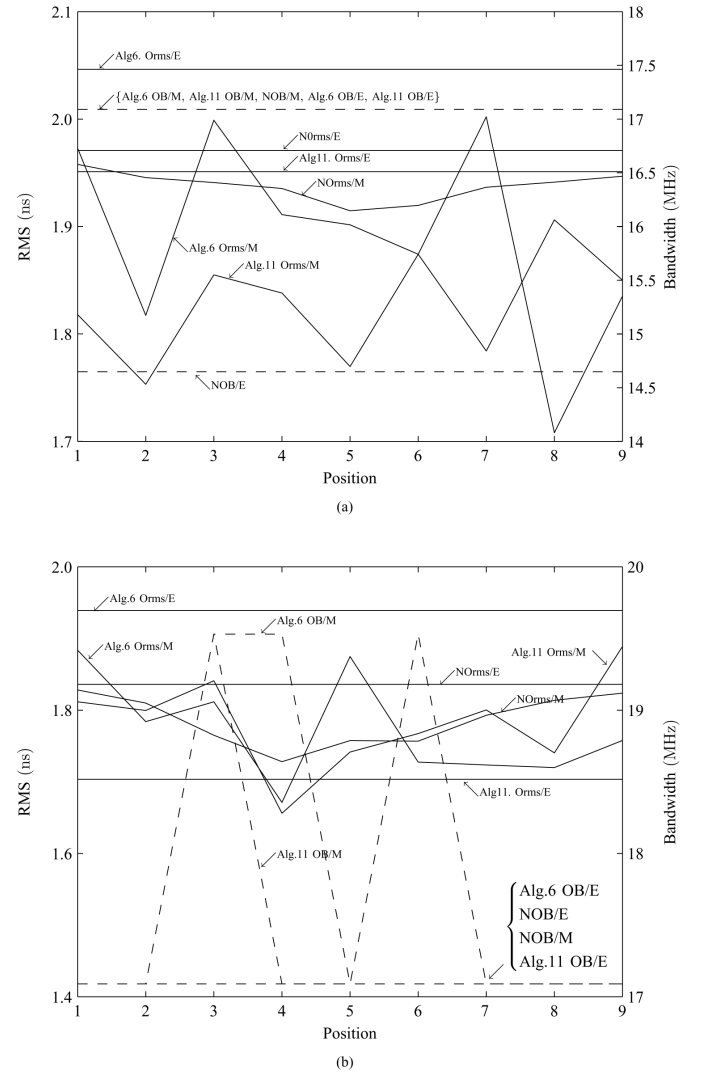

Fig. 9. Bandwidth and rms delay spread in two dynamic environments. (a) Environment 1, movement pattern 1. (b) Environment 2, movement pattern 2.

the received power distribution in multiple dynamic environments. Careful analysis of the GA performance has resulted in several relationships between population size, selection scheme, mutation rate and genotype structure. Two algorithms in particular have been highlighted as possible candidates for a final application solution. In an empty room algorithm 6 produced a highly repeatable improvement in the power distribution, reducing deviation by up to 24%, whilst algorithm 11 produced marginally lower improvements, but benefited from being a much more practical algorithm to implement. In the mobile scenarios shown, the GA managed to reduce power deviation by up to 26%, and forming, while the user perturbed the channel, a consistent power distribution to within 12%. Furthermore, the optimisation of the power distribution was carried out with only negligible impact to bandwidth and rms delay spread. Based upon the simulation conducted, work could be carried out on producing a optimal receiver design with regards to complexity, power efficiency and cost, using a $\text{FOV}_{\mathcal{R}_j} = 55°$ for mass product integration.

REFERENCES

[1] F. R. Gfeller and U. Bapst, "Wireless in-house data communication via diffuse infrared radiation," *Proc. IEEE*, vol. 67, no. 11, pp. 1474–1486, 1979.

[2] A. J. C. Moreira, R. T. Valadas, and A. M. de Oliveira Duarte, "Optical interference produced by artificial light," *Wirel.Netw.*, vol. 3, no. 2, pp. 131–140, 1997.

[3] H. Hashemi, G. Yun, M. Kavehrad, F. Behbahani, and P. A. Galko, "Indoor propagation measurements at infrared frequencies for wireless local area networks applications," *IEEE Trans. Veh. Technol.*, vol. 43, no. 3, pp. 562–576, 1994.

[4] D. C. O'Brien, M. Katz, P. Wang, K. Kalliojarvi, S. Arnon, M. Matsumoto, R. J. Green, and S. Jivkova, "Short range optical wireless communications," *Wireless World Research Forum*, 2005.

[5] P. Djahani and J. M. Kahn, "Analysis of infrared wireless links employing multibeam transmitters and imaging diversity receivers," *IEEE Trans. Commun.*, vol. 48, no. 12, pp. 2077–2088, 2000.

[6] R. Ramirez-Iniguez and R. J. Green, "Optical antenna design for indoor optical wireless communication systems," *Int. J. Commun. Syst.*, vol. 18, no. 3, pp. 229–245, 2005.

[7] M. F. L. Abdullah, "Techniques for signal to noise ratio adaptation in infrared optical wireless for optimisation of receiver performance," Ph.D. dissertation, 2007.

[8] D. C. M. Lee, J. M. Kahn, and M. D. Audeh, "Trellis-coded pulse-

position modulation for indoor wireless infrared communications," *IEEE Trans. Commun.*, vol. 45, no. 9, pp. 1080–1087, 1997.

[9] H. Uno, K. Kumatani, H. Okuhata, I. Shirakawa, and T. Chiba, "ASK digital demodulation scheme for noise immune infrared data communication," *Wirel.Netw.*, vol. 3, no. 2, pp. 121–129, 1997.

[10] R. J. Dickenson and Z. Ghassemlooy, "A feature extraction and pattern recognition receiver employing wavelet analysis and artificial intelligence for signal detection in diffuse optical wireless communications," *IEEE Trans. Wireless Commun.*, vol. 10, no. 2, pp. 64–72, 2003.

[11] S. Kirkpatrick, C. D. Gelatt, and M. P. Vecchi, "Optimization by simulated annealing," *Science*, vol. 220, no. 4598, pp. 671–680, 1983.

[12] D. W. K. Wong, G. Chen, and J. Yao, "Optimization of spot pattern in indoor diffuse optical wireless local area networks," *Opt. Express*, vol. 13, no. 8, pp. 3000–3014, 2005.

[13] M. Wen, J. Yao, D. W. K. Wong, and G. C. K. Chen, "Holographic diffuser design using a modified genetic algorithm," *Opt.Eng.*, vol. 44, no. 8, pp. 085 801–8, 2005.

[14] P. L. Eardley, D. R. Wisely, D. Wood, and P. McKee, "Holograms for optical wireless lans," *IEE Proc. Optoelectron.*, vol. 143, no. 6, pp. 365–369, 1996.

[15] A. G. Al-Ghamdi and J. M. H. Elmirghani, "Analysis of diffuse optical wireless channels employing spot-diffusing techniques, diversity receivers, and combining schemes," *IEEE Trans. Commun.*, vol. 52, no. 10, pp. 1622–1631, 2004.

[16] H. Yang and C. Lu, "Infrared wireless lan using multiple optical sources," *IEE Proc. Optoelectron.*, vol. 147, no. 4, pp. 301–307, 2000.

[17] V. Pohl, V. Jungnickel, and C. von Helmolt, "Integrating-sphere diffuser for wireless infrared communication," *IEE Proc. Optoelectron.*, vol. 147, no. 4, pp. 281–285, 2000.

[18] T. Komine and M. Nakagawa, "Fundamental analysis for visible-light communication system using led lights," *IEEE Trans. Consum. Electron.*, vol. 50, no. 1, pp. 100–107, 2004.

[19] S. Jivkova, B. A. Hristov, and M. Kavehrad, "Power-efficient multispot-diffuse multiple-input-multiple-output approach to broad-band optical wireless communications," *IEEE Trans. Veh. Technol.*, vol. 53, no. 3, pp. 882–889, 2004.

[20] D. C. O'Brien, G. E. Faulkner, E. B. Zyambo, K. Jim, D. J. Edwards, P. Stavrinou, G. Parry, J. Bellon, M. J. Sibley, V. A. Lalithambika, V. M. Joyner, R. J. Samsudin, D. M. Holburn, and R. J. Mears, "Integrated transceivers for optical wireless communications," *IEEE J. Sel. Topics. Quantum Electron.*, vol. 11, no. 1, pp. 173–183, 2005.

[21] C. R. Lomba, R. T. Valadas, and A. M. O. Duarte, "Experimental characterisation and modelling of the reflection of infrared signals on indoor surfaces," *IEE Proc. Optoelectron.*, vol. 145, pp. 191–197, 1998.

[22] B. T. Phong, "Illumination for computer generated pictures," *Commun ACM*, vol. 18, no. 6, pp. 311–317, 1975.

[23] S. R. Perez, R. P. Jimenez, F. J. L. Hernandez, O. B. G. Hernandez, and A. J. A. Alfonso, "Reflection model for calculation of the impulse response on ir-wireless indoor channels using ray-tracing algorithm," *Microwave. Opt. Technol. Lett.*, vol. 32, no. 4, pp. 296–300, 2002.

[24] J. M. Kahn, W. J. Krause, and J. B. Carruthers, "Experimental characterization of non-directed indoor infrared channels," *IEEE Trans. Commun.*, vol. 43, no. 234, pp. 1613–1623, 1995.

[25] J. R. Barry, J. M. Kahn, W. J. Krause, E. A. Lee, and D. G. Messerschmitt, "Simulation of multipath impulse response for indoor wireless optical channels," *IEEE J. Sel. Areas Commun.*, vol. 11, no. 3, pp. 367–379, 1993.

[26] J. B. Carruthers, S. M. Carroll, and P. Kannan, "Propagation modelling for indoor optical wireless communications using fast multi-receiver channel estimation," *IEE Proc., Optoelectron.*, vol. 150, no. 5, pp. 473–481, 2003.

[27] J. B. Carruthers and P. Kannan, "Iterative site-based modeling for wireless infrared channels," *IEEE Trans. Antennas Propag.*, vol. 50, no. 5, pp. 759–765, 2002.

[28] J. B. Carruthers and J. M. Kahn, "Modeling of nondirected wireless infrared channels," *IEEE Trans. Commun.*, vol. 45, no. 10, pp. 1260–1268, 1997.

[29] *BS EN 60825-1:1994: Safety of laser products. Equipment classification, requirements and user's guide*, Std.

[30] A. C. Boucouvalas, "IEC 825-1 eye safety classification of some consumer electronic products," *IEE Seminar Digests*, vol. 1996, no. 32, pp. 13/1–13/6, 1996.

[31] I. Haratcherev, J. Taal, K. Langendoen, R. Lagendijk, and H. Sips, "Automatic ieee 802.11 rate control for streaming applications," *Wireless Commun. Mob. Comput.*, vol. 5, no. 4, pp. 421–437, 2005.

[32] A. Garcia-Zambrana and A. Puerta-Notario, "Novel approach for increasing the peak-to-average optical power ratio in rate-adaptive optical wireless communication systems," *IEE Proc., Optoelectron.*, vol. 150, no. 5, pp. 439–444, 2003.

[33] M. R. Pakravan and M. Kavehrad, "Indoor wireless infrared channel characterization by measurements," *IEEE Trans. Veh. Technol.*, vol. 50, pp. 1053–1073, 2001.

[34] T. Bäck, U. Hammel, and H. P. Schwefel, "Evolutionary computation: Comments on the history and current state," *IEEE Trans. Evol. Comput.*, vol. 1, no. 1, pp. 3–17, 1997.

[35] F. Rothlauf, *Representations for genetic and evolutionary algorithms*. Physica-Verlag, 2002.

[36] F. O'Karray and C. W. D. Silva, *Soft computing and intelligent systems design : theory, tools, and applications*. Pearson/Addison Wesley, 2004.

[37] T. Bäck, *Evolutionary algorithms in theory and practice : evolution strategies, evolutionary programming, genetic algorithms*. Oxford University Press, 1996.

[38] J. E. Baker, "Reducing bias and inefficiency in the selection algorithm," in *Proc. 2nd Int. Conf. Genetic Algorithms and their application*, 1987.

[39] R. Poli, "Tournament selection, iterated coupon-collection problem, and backward-chaining evolutionary algorithms," in *Foundations of Genetic Algorithms*, 2005, pp. 132–155.

[40] A. G. Al-Ghamdi and J. M. H. Elmirghani, "Analysis of optical wireless links employing a beam clustering method and diversity receivers," in *IEEE Int. Conf. Commun.*, vol. 6, 2004, pp. 3341–3347.

[41] G. Yun and M. Kavehrad, "Spot-diffusing and fly-eye receivers for indoor infrared wireless communications," in *IEEE Int. Conf. Sel. Topics Wireless Commun.*, 1992, pp. 262–265.

[42] A. S. Glassner, "Space subdivision for fast ray tracing," *IEEE Comput. Graph. Appl.*, vol. 4, no. 10, pp. 15–22, 1984.

Matthew D. Higgins received his MEng degree in Electronic and Communications Engineering in 2005 from the University of Warwick, UK, and is currently working towards his PhD at the same institution. His major area of research is focused on mobile optical wireless communications systems, specifically the use of genetic algorithms for channel optimisation, and the application of nonlinear devices for receiver technology. Matthew is a Member of the IET and Student Member of both the IEEE and SPIE.

Roger J. Green became Professor of Electronic Communication Systems at Warwick in September 1999, and Head of the Division of Electrical and Electronic Engineering in August 2003. He has published over 190 papers in the field of optical communications, optoelectronics, video and imaging, and has several patents. Some 46 PhD research students have worked successfully under his supervision. He leads the Communications and Signal Processing Research Group, which is the largest in the School of Engineering at Warwick. His current interests include optical detection systems in communications and imaging technology. He is a Fellow of the IET and has served on IEE committee E14. He is also a Senior Member of the IEEE, and currently serves on two IEEE committees concerned with communications and signal processing. He has been a member of the EPSRC College since 2002, and is a member of the Engineering Professors' Council. He has formed two Warwick spin-offs - Shibden Limited and Optical Antenna Solutions.

Mark S. Leeson received a PhD from the University of Cambridge, UK, in 1990 and then worked as a Network Analyst for a UK bank until 1992. Subsequently, he held several academic appointments before joining the University of Warwick in March 2000, where he is now an Associate Professor. His major research interests are optical receivers, optical communication systems, communication protocols, ad hoc networking and evolutionary optimization. To date he has over 100 publications in these fields and is a Chartered Member of the UK Institute of Physics.